A&A 470, 211–219 (2007)
DOI: 10.1051/0004-6361:20066108

Astronomy & Astrophysics

The outburst of the eruptive young star OO Serpentis between 1995 and 2006⋆,⋆⋆

Á. Kóspál[1], P. Ábrahám[1], T. Prusti[2], J. Acosta-Pulido[3], S. Hony[4], A. Moór[1], and R. Siebenmorgen[5]

[1] Konkoly Observatory of the Hungarian Academy of Sciences, PO Box 67, 1525 Budapest, Hungary
e-mail: kospal@konkoly.hu
[2] ESTEC/SCI-SAF, Postbus 299, 2200 AG Noordwijk, The Netherlands
[3] Instituto de Astrofísica de Canarias, 38205 La Laguna, Tenerife, Canary Islands, Spain
[4] Instituut voor Sterrenkunde, K.U. Leuven, Celestijnenlaan 200B, 3001 Leuven, Belgium
[5] European Southern Observatory, Karl-Schwarzschild-Strasse 2, 85748 Garching, Germany

Received 25 July 2006 / Accepted 22 April 2007

ABSTRACT

Aims. OO Serpentis is a deeply embedded pre-main sequence star in the Serpens NW star-forming region. The star went into outburst in 1995 and gradually faded afterwards. In many respects its eruption resembled the well-known FU Orionis-type (FUor) or EX Lupi-type (EXor) outbursts. Since very few such events have ever been documented at infrared wavelengths, our aim is to study the temporal evolution of OO Ser in the infrared.

Methods. OO Ser was monitored with the *Infrared Space Observatory* in the 3.6–100 μm wavelength range, starting 4 months after peak brightness and covering a period of 20 months. Eight years later, in 2004-2006 we again observed OO Ser at 2.2 and 12 μm from the ground and complemented this dataset with archival Spitzer observations also from 2004. We analysed these data with special attention to source confusion and constructed light curves at 10 different wavelengths as well as spectral energy distributions.

Results. The outburst caused brightening in the whole infrared regime. According to the infrared light curves, OO Ser started a wavelength-independent fading after the peak brightness. Later the flux decay became slower but stayed practically wavelength-independent. The fading is still ongoing, and current fading rates indicate that OO Ser will not return to quiescent state before 2011. The outburst timescale of OO Ser seems to be shorter than that of FUors, but longer than that of EXors.

Conclusions. The outburst timescale and the moderate luminosity suggest that OO Ser is different from both FUors and EXors, and shows some similarities to the recently erupted young star V1647 Ori. Based on its SED and bolometric temperature, OO Ser seems to be an early class I object, with an age of $<10^5$ yr. As proposed by outburst models, the object is probably surrounded by an accretion disc and a dense envelope. This picture is also supported by the wavelength-independence of the fading. Due to the shorter outburst timescales, models developed for FUors can only work for OO Ser if the viscosity parameter in the circumstellar disc, α, is set to an order of magnitude higher value than usual for FUors.

Key words. stars: pre-main sequence – stars: circumstellar matter – infrared: stars – stars: individual: OO Serpentis

1. Introduction

OO Serpentis ($\alpha_{2000} = 18^{\rm h}29^{\rm m}49\overset{\rm s}{.}1$, $\delta_{2000} = +01°16'20''$) is a deeply embedded pre-main sequence star in the Serpens NW star-forming region at a distance of 311 pc. In 1995 OO Ser underwent a large increase in K-band flux in less than 1 year, reaching its maximum brightness in 1995 October (Hodapp et al. 1996b). The object was not visible, even at peak brightness, in the J-band or at shorter wavelengths, therefore it is also known as Serpens Deeply Embedded Outburst Star (DEOS). In the H and K bands the object was observable but the emission is dominated by scattered light. In the K-band Hodapp (1999) monitored the outburst until 1998 October, and found that after the peak OO Ser gradually faded at a rate faster than the typical fading rate of FU Orionis-type objects (FUors), but slower than that of EX Lupi-type stars (EXors). Its K-band spectrum (a steeply rising, smooth continuum) also differed from both FUor and EXor spectra, which usually exhibit absorption or emission features.

Eruptions of pre-main sequence stars are rare events, thus a new outburst is always noteworthy. The eruption mechanism is thought to be caused by enhanced accretion from the circumstellar disc onto the star (e.g. Hartmann & Kenyon 1996). The close link between the eruption phenomenon and the circumstellar material makes it crucial to document the outburst also at infrared wavelengths, where the circumstellar dust radiates. However, such observing programmes are constrained by the availability of active infrared satellite missions. The physical analysis of the phenomenon is limited due to the lack of preoutburst data. The eruption of OO Ser in 1995 provided a unique opportunity to collect such a dataset and carry out a multiwavelength infrared study of the whole outburst event for the first time.

Triggered by the news on the outburst of OO Ser we activated a Target of Opportunity programme on the *Infrared Space Observatory* (ISO, Kessler et al. 1996). The infrared monitoring started 4 months after the maximum brightness of OO Ser, and continued for 20 months. The ISO-SWS measurements from this programme were published separately by Larsson et al. (2000). They found that OO Ser changed its infrared fluxes in

⋆ Based on observations with ISO, an ESA project with instruments funded by ESA member states (especially the PI countries France, Germany, the Netherlands and the UK) with participation of ISAS and NASA.

⋆⋆ Tables 1 and 2 are only available in electronic form at http://www.aanda.org

the 2−45 μm range and estimated an extinction of $A_V \approx 20$ mag from the optical depth of the 10 μm silicate absorption feature. In an independent programme the Serpens core was surveyed by the ISOCAM instrument providing 6.7 and 14.3 μm photometry on OO Ser for a single epoch (Kaas et al. 2004).

In this paper we analyse our ISOPHOT and ISOCAM observations from the monitoring programme. In addition to ISO measurements, we observed OO Ser from the ground at 2.2 μm in 2004 and 2006 as well as at 12 μm in 2004. We complemented this database with archival Spitzer data also from 2004, as well as with previously published measurements on OO Ser from the literature.

2. Observations and data reduction

2.1. ISOPHOT observations

ISOPHOT, the photometer on-board ISO (Lemke et al. 1996), carried out multi-filter photometry with 9 different filters in the 3.6−200 μm wavelength range and spectrophotometry in the 2.47−11.62 μm range, at 8 different epochs between 1996 February and 1997 September. Table 1 shows the log of the observations. In most cases small raster maps were obtained except in 1997 September, when at 25 μm and shortwards the source and background positions were observed separately. The typical integration time was 64 s. Aperture sizes varied according to the filters: 13.″8 at 3.6 μm, 18″ at 4.8 μm, 52″ at 12, 15 and 25 μm. At 60 and 100 μm the C100 camera (3 × 3 pixel, 43″ × 43″ per pixel), while at 170 and 200 μm the C200 camera (2 × 2 pixel, 89″ × 89″ per pixel) was utilised. Some far-infrared observations were performed in the PHT 32 mode, which provided higher spatial resolution (for a description of this mode see Tuffs & Gabriel 2003).

2.2. ISOPHOT data processing

Standard processing and absolute flux calibration. The data reduction was performed using the ISOPHOT Interactive Analysis Software Package V10.0 (PIA, Gabriel et al. 1997). The integration ramps were corrected for non-linearities. Cosmic particle hits were removed using the two thresholds deglitching method, and signal values were derived by fitting a first order polynomial to each ramp. The signals were transformed to a standard reset interval, then an orbital dependent dark current was subtracted and cosmic ray hits were again checked. In case the signal did not fully stabilise during the measurement time due to detector transients, only the last part of the data stream was used. This was found mainly in observations with the 12 and 25 μm filters, while at other wavelengths the measurements showed sufficient stability. The absolute flux calibration of measurements at 25 μm and shortwards was done by adopting the default responsivity of the detector. The ISOPHOT Handbook (Laureijs et al. 2003) gives a typical absolute flux uncertainty of 40% at 3.6, 4.8, 12 and 15 μm, and 10% at 25 μm for ON/OFF staring measurements. Since our small raster maps enabled better background subtraction than the ON/OFF mode, the error of our measurements is probably smaller. Nevertheless, we adopted the abovementioned values as conservative estimates for the absolute flux uncertainty (see Col. 9 of Table 1).

Relative flux determination. Due to the monitoring strategy, the observations were carried out with the same instrument setup at most epochs. This enabled us to determine relative flux variations at a certain wavelength more accurately than the standard processing by applying a new method developed at Konkoly Observatory especially for the fine relative calibration of ISOPHOT data (Juhász et al. 2007). The algorithm compares the detector transient curves in a measurement sequence with the corresponding curves of a reference day (in our case 1996 October 24) and determines a scaling factor between the signals of the two epochs. Evaluating all epochs, one obtains a light curve normalized to the reference day. The final fluxes are computed as the product of the scaling factors and the absolute flux level of the reference day. The method provides relative uncertainties, which correspond to the formal errors of the scaling factors. In our case, the relative uncertainties were usually around or below 10% (see Col. 10 of Table 1). The absolute flux level of the whole light curve is determined by the absolute calibration of the reference flux.

Far-infrared maps. The far-infrared observations at 60 and 100 μm were processed with PIA in a standard way. PHT32 observations at 170 and 200 μm were reduced using a dedicated software package (P32TOOLS) developed at MPI Kernphysik in Heidelberg (Tuffs & Gabriel 2003). This tool provides adequate correction for transients in PHT32 measurements. Absolute calibration was done by comparing the source flux with the on-board fine calibration source. At 60 and 100 μm each 9 × 3 map was flat-fielded using the first raster step (3 × 3 pixel) as the sky flat position. Then the sum of two point spread functions, centred on the positions of OO Ser and a nearby submillimetre source, SMM 1 (see Sect. 2.7), was fitted to the brightness distribution on the map using the ISOPHOT measured footprint maps. A similar fitting procedure was applied to the PHT32 maps. The errors given in Table 1 represent the quadratic sum of the formal uncertainties of the fits (in the range of 3−15%) and the photometric calibration uncertainty of the detector given in the ISOPHOT Handbook (Laureijs et al. 2003). We note that with this technique OO Ser could be separated from SMM 1 but not from other closer nearby sources, which may contaminate the flux of OO Ser. 9 × 3 maps at 60 and 100 μm were obtained at 7 different epochs, but the first two measurements (in 1996 February and April) were executed at late orbital phases during ISO's orbit. This caused a large uncertainty in these measurements, thus we decided not to present them. In the PHT32 oversampled maps more than one detector pixel observed OO Ser; their independent photometric results were combined with a robust averaging technique described by Ábrahám et al. (2004a).

ISOPHOT-S. Spectrophotometric observations, also in the form of 3 × 1 small raster maps centred on OO Ser, were obtained with the ISOPHOT-S subinstrument. The processing of these data deviated from the standard scheme implemented in PIA. ISOPHOT-S has a successful dynamic calibration for staring observations but in PIA this method is not applicable for rasters, leading to uncorrected transients and consequently reduced photometric accuracy. Since the contrast between OO Ser and the background level is relatively low, we treated these rasters as long staring observations, and applied the dynamic calibration by modifying some PIA routines. The resulting photometric uncertainties are in the range of 5−10%.

Colour corrections. Colour corrections were applied to each broadband photometric measurement by convolving the

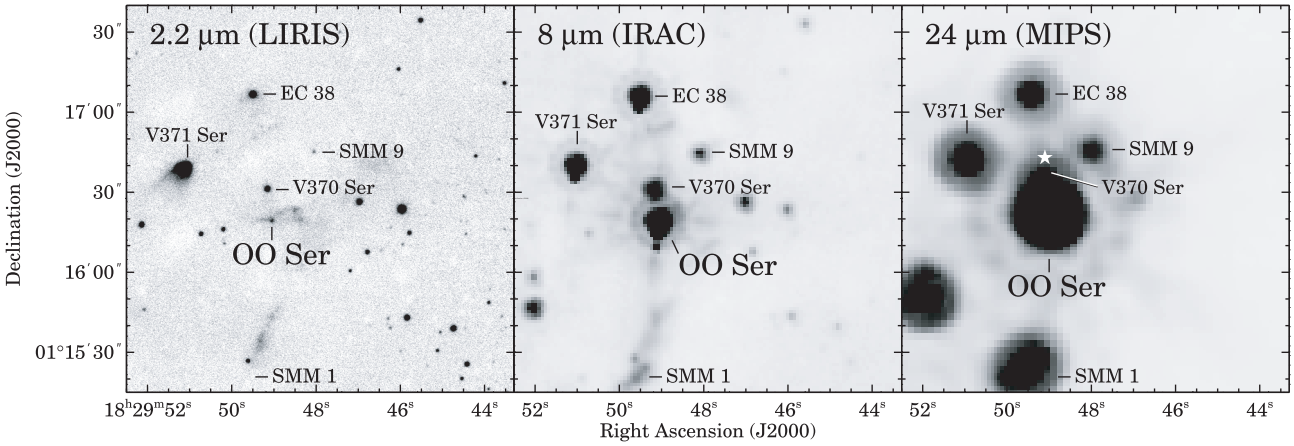

Fig. 1. OO Ser and its surroundings at different infrared wavelengths. V370 Ser (EC 37), V371 Ser (EC 53), EC 38, SMM 9 and SMM 1 are also marked. In the middle panel, the spots below the brightest sources are instrumental artifacts ("bandwidth effects"). The white star in the right panel indicates the position of IRAS 18272+0114 as given in the IRAS Catalog of Point Sources.

observed spectral energy distribution (SED) at a certain epoch with the ISOPHOT filter profile in an iterative way. The result of the ISOPHOT photometry is presented in Table 1.

2.3. ISOCAM observations and data processing

The 6.7 and 14.3 μm photometry was obtained with the ISOCAM instrument (Cesarsky et al. 1996) on 1997 September 22 (see Table 1). The data were reduced with the CAM Interactive Analysis Software V5.0 (CIA, Ott et al. 1997). A dark current correction was applied following the "VilSpa" method. Glitches were removed using the "multiresolution median transform". This efficiently removes glitches based on the fact that glitches in general are much shorter than the signature of a real source. The data were stabilised using the Fouks-Schubert model. Next the individual frames were averaged to four mean images, one for each sky position. After this, a second deglitching was applied based on the overlapping projected sky positions of these mean images. Finally, the images were flat-fielded and combined into the final mosaic. The pixel values were converted to mJy/arcsec^2 using the tabulated conversion factors available in CIA.

Photometry of the sources was obtained using the IRAF tool "xphot". We used a small aperture photometry of 4.″5 and 6″ radius for the 6.7 and 14.3 μm mosaic, respectively. These values were then corrected for the flux falling in the wings of the point spread function outside the chosen aperture. The small aperture was selected because of a nearby source (V370 Ser at a distance of ∼11″) which otherwise would have contributed to the measured flux. The results are shown in Table 1. The insignificant background level of 1 and 3 mJy/arcsec^2 does not contribute to the measurement error, which should be dominated by the absolute flux calibration uncertainty of 3.3% at 6.7 μm and 4.8% at 14.3 μm (Blommaert et al. 2003).

2.4. Near-infrared observations and data processing

K_S-band images were obtained by the LIRIS instrument on 2004 June 11 (as part of the LIRIS Guaranteed Time programme) and on 2006 May 6. LIRIS is an infrared camera/spectrograph built at the Instituto de Astrofísica de Canarias (Acosta-Pulido et al. 2003; Manchado et al. 2004), and is mounted on the 4.2 m William Herschel Telescope at the Observatorio del Roque de los Muchachos (Canary Islands). The detector used is a 1024 × 1024 HAWAII–1 detector (Hodapp et al. 1996a), which provides a plate scale of 0.″250/pixel and a total area of 4.′27 × 4.′27. In 2004 a three point dither pattern was used with a total exposure time of 140 s, while in 2006 a five-point dither pattern was used and the total exposure time was 250 s. The images were reduced using the IRAF package "liris_ql" developed by the LIRIS team within the IRAF environment. The reduction steps consist of flat-fielding, sky subtraction and image co-addition.

In Fig. 1 (left) a part of our K_S-band LIRIS image from 2004 can be seen showing the surroundings of OO Ser. The eruptive star was clearly detected in K_S and a faint nebulosity around the star can be seen as well (see also Sect. 3.1). Because of this nebulosity, photometry should be done carefully. In order to be able to compare our measurements with those of Hodapp (1999), we used an aperture diameter of 11.″3, the same as Hodapp (1999). Conversion from instrumental magnitudes to real magnitudes was done using the 2MASS $J-K_S$ colour versus ΔK_S (the difference between the instrumental and the 2MASS K_S magnitudes) relationship for 20 comparison stars in the field. The resulting values are $K_S = 14.3 \pm 0.2$ mag in 2004 and $K_S = 14.1 \pm 0.2$ mag in 2006. We note that the colours of the 20 comparison stars used in this calibration procedure covered a large enough range to include also the colour of OO Ser itself. Similar photometry was derived for some nearby sources (similarly to Hodapp 1999, we used a larger, 11.″3 diameter aperture for the two extended objects: OO Ser and V371 Ser, and a smaller 1.″9 diameter aperture with the corresponding aperture correction for the point-like objects: V370 Ser, EC 38 and SMM 9); the results can be seen in Table 2.

A K-band spectrum of OO Ser was obtained using LIRIS on 2006 May 6. The observation was performed following an ABBA telescope nodding pattern. The total exposure time was 2400 s, split in 4 individual exposures of 600 s. In order to reduce the readout noise, the measurements were done using multiple correlated readout mode, with 4 readouts before and after the integration. We used a slit width of 1″ and a medium resolution sapphire grism which yielded a spectral resolution of 2500. The wavelength calibration was provided by observations of an Argon lamp available in the calibration unit at the A&G box of the telescope. In order to obtain the telluric correction, the nearby A0V star HIP 90123 was observed with the same configuration as the object. The data were reduced and calibrated

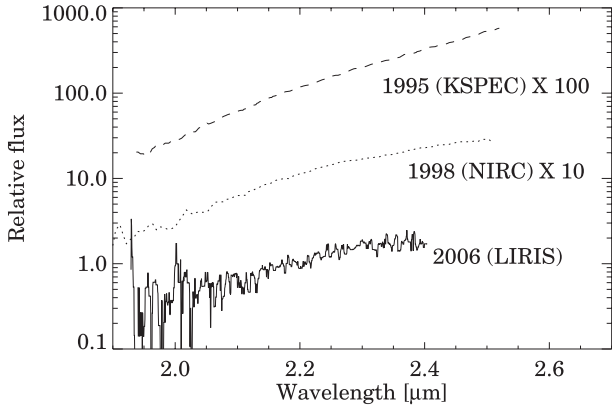

Fig. 2. Normalised K-band spectra of OO Ser. *Continuous line*: this work, *dashed and dotted lines*: Hodapp (1999). For clarity, we multiplied the spectrum from 1998 by 10 and the spectrum from 1995 by 100.

using the package "liris_ql". Consecutive pairs of AB two-dimensional images were subtracted to remove the sky background, then the resulting images were wavelength calibrated and flat-fielded before registering and coadding all frames to provide the final combined spectrum. A one-dimensional spectrum was extracted with the IRAF "apall" task. The extracted spectrum was divided by a composite to eliminate telluric contamination. This composite spectrum was generated from the observed spectrum of the calibration star, divided by a stellar model and convolved to our spectral resolution. The resulting normalised K-band spectrum is shown in Fig. 2.

2.5. Mid-infrared observations and data processing

OO Ser was imaged with TIMMI2 mounted on the ESO 3.6 m telescope at La Silla on 2004 October 21, under clear and stable conditions. The N11.9-OCLI filter was used which has a central wavelength of 11.66 μm and a *FWHM* of 1.16 μm. The total integration time was 4 min. Both chopping and nodding amplitudes were 10″, and the 0.″2 pixel scale of the 240 × 320 Raytheon detector was set. This resulted in a chop-nod corrected image with two negative and two positive beams captured on the detector. The four beams were used for independent determination of the source flux and error. The resulting fluxes are 0.64 Jy for OO Ser and 0.18 Jy for V370 Ser (a nearby young star also visible in the field, see also Table 2). The flux calibrator was the photometric standard HD 96171 which was observed with the same set-up. Other photometric standard star observations of the same night were inspected to estimate the total absolute flux uncertainty of ∼15%.

2.6. Spitzer observations and data processing

OO Ser was measured with the IRAC and MIPS instruments of the Spitzer Space Telescope on 2004 April 4 and 5, respectively, as part of the legacy programme "c2d" (PI: Neal J. Evans II). The third data release of this programme containing enhanced data products and catalogues can be downloaded from the Spitzer website[1]. As an example we plotted parts of the 8 μm IRAC and the 24 μm MIPS maps in Fig. 1.

The "c2d" catalogue contains IRAC fluxes for OO Ser, but it is treated as a point source. The nebulosity seen in the K-band images, however, are still visible at 3.6 and 4.5 μm too. In order to be able to compare the IRAC fluxes with the ISO measurements, we decided to extract fluxes from the IRAC images for OO Ser using the same apertures as ISOPHOT used (diameter of 13.″8 at 3.6 μm and 18″ at ≥4.5 μm)

The current version of the "c2d" catalogue does not contain MIPS fluxes yet. In order to obtain photometry in the MIPS bands, we downloaded the enhanced MIPS images. At 24 μm we selected 7 isolated stars to construct the point spread function. Since OO Ser was saturated, this profile was then fitted to the non-saturated wings of OO Ser. At 70 μm OO Ser and a nearby young star, V370 Ser could not be fully separated. Thus an aperture of 20″ was utilized, which included both objects. The measured flux was then distributed between OO Ser and V370 Ser in the same ratio as their peak brightnesses (measured in a 5″ aperture at the position of the two sources). We also extracted 70 μm photometry for some other sources in the vicinity of OO Ser, since they possibly cause source confusion in IRAS and ISO far-infrared measurements. In these cases, a 20″ aperture was utilized with a fixed 0.142 Jy background.

Colour corrections were applied to each measurement for each source by convolving the observed SED with the IRAC and MIPS filter profiles in an iterative way. The resulting fluxes and estimated uncertainties can be seen in Table 2.

2.7. Source confusion

Figure 1 shows that several infrared and submillimetre sources are present in the vicinity of OO Ser: V370 Ser (also known as EC 37), V371 Ser (also known as EC 53 or SMM 5), EC 38, SMM 9 and SMM 1. At shorter wavelengths (2.2, 3.6, 4.5 and 5.8 μm) an extended nebulosity around OO Ser can also be seen. Thus, when comparing the fluxes of OO Ser measured with different instruments one has to keep in mind that – to some extent – the nebulosity and some of the abovementioned sources may contribute to the observed flux at a particular wavelength. At 2.2 μm and with the ISOPHOT/ISOCAM at 3.6, 4.8, 6.7 and 14.3 μm the beams included OO Ser only. At 12, 15 and 25 μm the ISOPHOT beams included OO Ser and V370 Ser. At 60, 100, 170 and 200 μm the fluxes extracted for OO Ser include also contributions from V370 Ser, V371 Ser, EC 38 and SMM 9. Recent infrared photometry for these sources can be seen in Table 2. It should be noted that fluxes presented in Table 1 contain the contributions of nearby sources as discussed above. In Sect. 3.4 we give a detailed description of how we corrected the ISOPHOT measurements for the effects of source confusion.

3. Results

3.1. Morphology of the nebula

According to Hodapp (1999) before the outburst a triangle-shaped nebula west of OO Ser and a small elongated nebula east of OO Ser could be seen. During the outburst these – presumably reflection – nebulae became much brighter. In this phase Hodapp et al. (1996b) observed OO Ser in the L' and M' bands, as well as at 11.7 and 20.6 μm. They found that the nebulosity can be seen in the L' but not at longer wavelengths. Our recent K_S-band images reveal that the nebulae still exist and look very similar to the preoutburst image of Hodapp (1999, see his Fig. 1 left). The nebulosity around OO Ser is also visible in the Spitzer/IRAC maps from 2004 at 3.6, 4.5 and 5.8 μm and some extended emission can be suspected even at 8 μm.

[1] http://ssc.spitzer.caltech.edu/legacy/all.html

3.2. Preoutburst fluxes

In order to study the consequences of the outburst in the whole infrared regime, one has to compile first the SED of OO Ser in the quiescent phase, i.e. estimate the preoutburst fluxes. At 2.2 μm there exists a preoutburst measurement from 1994 (Hodapp et al. 1996b). At longer wavelengths, only the IRAS measurements are available from 1983. Analysing high-resolution IRAS maps, Hurt & Barsony (1996) derived fluxes of 0.63, 4.5, 24 and 111 Jy at 12, 25, 60 and 100 μm, respectively. The authors claim that these values represent the total fluxes from a region encompassing three confused sources: OO Ser, V371 Ser and SMM 9, and they give the one third of the abovementioned values as upper limits for the brightness of OO Ser. The position of IRAS18272+0114 from the IRAS Catalog of Point Sources (marked by a white star in Fig. 1 right) is located halfway between the sources, which may indicate that there was no dominant source, but all sources had comparable contributions to the IRAS flux.

With the help of Spitzer/MIPS measurements, it is possible to check the validity of the assumption of Hurt & Barsony (1996) via estimating the preoutburst fluxes of OO Ser at 25 and 60 μm. Assuming that EC 38 and SMM 9 have non-variable far-infrared fluxes, we subtracted the contribution of these sources from the IRAS values cited above. Another nearby source, V371 Ser, exhibits near-infrared variability of $\approx$1.5 mag and shares many characteristics with EXors (Hodapp 1999). At far-infrared wavelengths, however, eruptive young stars do not typically show significant flux changes (Ábrahám et al. 2004a). Thus we assumed that V371 Ser is also non-variable at 25 and 60 μm, at least within our measurement uncertainties, and we subtracted its flux from the IRAS values. In practice, we estimated 25 μm fluxes for these nearby sources via interpolating from the 24 μm MIPS values in Table 2, and subtracted the sum of these (3.6 Jy) from the value given by Hurt & Barsony (1996) (4.5 Jy). The result is 0.9 Jy, which is indeed of the order of one third of 4.5 Jy. The result at 60 μm is also roughly consistent with the one third value. Due to the lack of recent 12 or 100 μm data for all nearby sources, the same test cannot be done at these wavelengths. Therefore, for homogeneity, at all four IRAS wavelengths we adopted as preoutburst fluxes the one third values within a factor of 2 uncertainty: $0.21^{+0.21}_{-0.10}$ Jy at 12 μm, $1.5^{+1.5}_{-0.8}$ Jy at 25 μm, 8^{+8}_{-4} Jy at 60 μm, 37^{+37}_{-19} Jy at 100 μm. We note that OO Ser is the first eruptive young star where preoutburst fluxes are available in the whole infrared wavelength regime. Similar preoutburst data can be found only for one other young eruptive star, V1647 Ori (Ábrahám et al. 2004b).

3.3. Spectral energy distribution

In Fig. 3 the SED of OO Ser in the high (outburst) state from 1996 September is plotted with filled symbols. We attempted to correct for the effects of source confusion as described in details in Sect. 3.4. Thus, the resulting SED in Fig. 3 represents the flux from OO Ser alone at $\lambda \leq 60\,\mu$m. Due to high extinction the star is invisible at optical wavelengths and is very faint in the near-infrared regime. In the mid-infrared (3–25 μm) the SED is rising towards longer wavelengths. This wavelength regime is zoomed in Fig. 4, showing a broad silicate absorption feature at 9.7 μm, as well as several ice features, which also indicate high extinction. Measuring the optical depth of the 9.7 μm feature, and converting it to visual extinction assuming $A_V/\Delta\tau_{9.7} = 18.5$ (Draine 2003), we obtained $A_V = 42 \pm 5$ mag. This value is twice as large as the one measured by Larsson et al. (2000); the difference

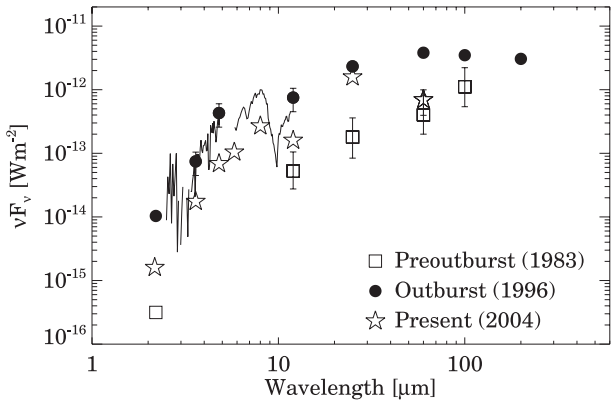

Fig. 3. Spectral energy distribution of OO Ser. *Squares*: preoutburst fluxes measured with IRAS in 1983 (Hurt & Barsony 1996), and *K*-band photometry from 1994 August, (Hodapp et al. 1996b); *Dots and line*: outburst fluxes from 1996 September, measured with ISOPHOT; *Stars*: current fluxes from 2004, measured with LIRIS, TIMMI2 and Spitzer. Error bars smaller than the symbol size are not plotted. ISOPHOT beams at 100 and 200 μm contained nearby sources; for a detailed discussion see Sects. 2.7 and 3.3.

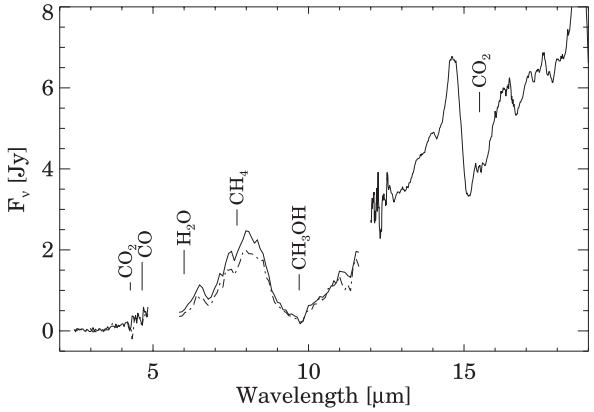

Fig. 4. Ice features in the spectrum of OO Ser. Data below 12 μm were taken by ISOPHOT-S. Solid line indicates data from 1996 October, dashed dot line from 1997 April. Data above 12 μm were taken by the ISO-SWS instrument (highly processed data products from Frieswijk et al. 2004). In order to obtain high signal-to-noise ratio, ISO-SWS spectra from 1997 March, April and September were averaged and a 0.3 μm wide moving median window was applied.

is probably related to the low signal-to-noise of his SWS spectra around the 9.7 μm absorption feature. The measured high extinction indicates that OO Ser is more deeply embedded than most FUors. At far-infrared wavelengths (60–200 μm) the SED is flat, but it should be noted that data points at 100 and 200 μm are contaminated by source confusion (see Sect. 2.7).

In Fig. 3 the preoutburst SED (see Sect. 3.2) and the present SED (based on measurements from 2004) are also plotted. They will be discussed in Sects. 3.4.2 and 3.4.6.

3.4. Light curves

ISOPHOT, ISOCAM, LIRIS, TIMMI2, Spitzer, IRAS (Hurt & Barsony 1996) and *K*-band measurements (Hodapp et al. 1996b; Hodapp 1999) were combined to construct the light curves of OO Ser at different wavelengths between 1995 and 2006.

For the subsequent light curve analyses, we attempted to correct for the effects of source confusion. One possibility would be to smooth all data to the same resolution, in most cases defined

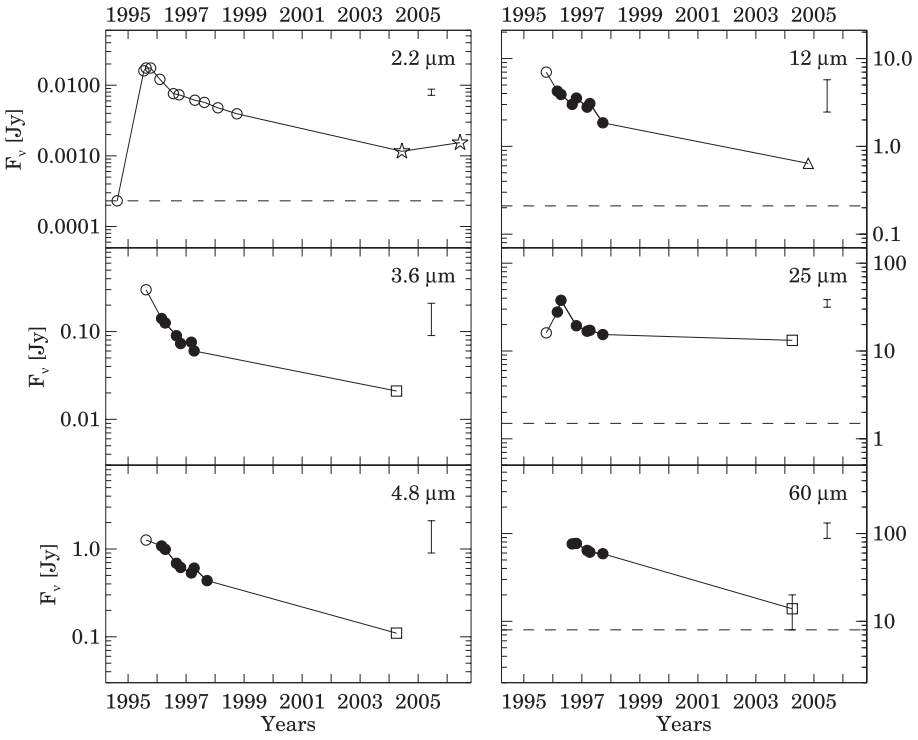

Fig. 5. Light curves of OO Ser at different wavelengths. *Open circles*: measurements of Hodapp et al. (1996b); Hodapp (1999); *Stars*: LIRIS; *Filled circles*: ISOPHOT; *Triangle*: TIMMI2; *Squares*: Spitzer; *Dashed lines*: preoutburst fluxes from 1994 at 2.2 μm and from 1983 at 12, 25 and 60 μm (for details see Sect. 3.2). Tick marks indicate January 1 of the corresponding year. Error bars in the upper right corner of each panel show the typical uncertainty in the absolute flux level. Due to the homogeneous measurement strategy, the uncertainties of the ISOPHOT data points relative to each other at a certain wavelength are usually better than the absolute errors (see Sect. 2.2). All fluxes are corrected for source confusion (for a detailed description see Sects. 2.7 and 3.4), thus these light curves show the brightness evolution of OO Ser alone.

by the ISOPHOT aperture. In doing so, however, several additional sources would be included in the beam, falsifying the fading rate calculations for OO Ser. Instead, we decided to use the higher spatial resolution images to correct for the contribution of additional, unrelated sources in the large ISOPHOT beams.

At 12 μm TIMMI2 could resolve OO Ser and V370 Ser. Assuming that V370 Ser is not variable at this wavelength, we subtracted its contribution of 0.18 Jy (see Table 2) from each ISOPHOT 12 μm measurement. The MIPS camera of Spitzer at 24 μm could separate OO Ser from V370 Ser giving a flux of 1.56 Jy for the latter source, which we interpolated to 25 μm (1.71 Jy) and subtracted from the ISOPHOT points at 25 μm. At 60 μm, MIPS 70 μm measurements could be utilized. Using the SEDs presented in Table 2, we interpolated 60 μm fluxes for V370 Ser, V371 Ser, EC 38 and SMM 9, and subtracted the sum of these values (24 Jy) from the ISOPHOT 60 μm data points. Due to the lack of 100 μm fluxes for the nearby sources, a similar correction was not possible in the case of the 100 μm ISOPHOT light curve.

In Fig. 5 six representative light curves between 2.2 and 60 μm are shown. All these light curves are corrected for source confusion and represent the brightness evolution of OO Ser alone. In the following, we describe these light curves in detail.

3.4.1. The outburst history at 2.2 μm

FUor and EXor ourbursts were historically monitored at optical wavelengths. Since OO Ser is invisible in the optical, K_S is the shortest available band where the outburst could have been followed. The top left panel of Fig. 5 shows the 2.2 μm light curve of OO Ser. The star brightened by 4.6 mag between 1994 August and 1995 July. After reaching peak brightness, it started an approximately exponential fading with a rate of 1.00 mag/year in the first 350 days and 0.34 mag/year afterwards, as the data between 1995 and 1999 indicate (Hodapp 1999). The change in fading rate divides this period of the outburst into a first and a second part. Our measurements from 2004−2006 prove that the fading continued, although at a slightly different rate, representing a third part of the fading. Comparing the preoutburst flux with the new observations, one can conclude that at 2.2 μm OO Ser is still above the preoutburst flux level.

In the following, we describe the lightcurves of OO Ser at longer wavelengths, following the abovementioned division: the initial rise (until peak brightness); the first part of the fading (until mid-1996); the second part of the fading (until mid-1997); and the third part of the fading (until 2004).

3.4.2. The initial rise (until peak brightness)

Comparison of the preoutburst fluxes with the SED in outburst (Fig. 3) shows that the eruption caused brightening in the whole near- to far-infrared spectrum. Although the fluxes at 100 μm are contaminated by nearby sources, there is a flux change at this wavelength, too. The shape of the SED changed significantly: the outburst SED is flatter.

At 2.2 μm the light curve reached its peak in 1995 October. At 3.6, 4.8 and 12 μm, the exact date of the peak is not known, but it happened not later than 1995 October, thus it was probably simultaneous with the K-band peak. At 25 μm, however, the peak took place in 1996 April, i.e. some 200 days later than at 2.2 μm. The shape of the peak at 25 μm is also different, it is broader than at 2.2 μm, and has a triangle-like shape. At 60 and 100 μm, the photometry is more uncertain, thus the peak dates cannot be determined. Nevertheless, the time-shift at 25 μm gives a hint that the peak brightness happened gradually later at longer wavelengths. To our knowledge, such a time-shift has not been observed for other eruptive stars.

In order to analyse the wavelength dependence of the brightening, in Fig. 6 we plotted the ratio of the peak flux to the preoutburst value at 2.2, 12, 25, 60 and 100 μm. Since at 100 μm both the preoutburst IRAS flux and the peak ISOPHOT flux include contributions from several nearby sources, the ratio derived from these numbers represents a lower limit for the brightening of OO Ser itself. Figure 6 suggests that the amplitude of

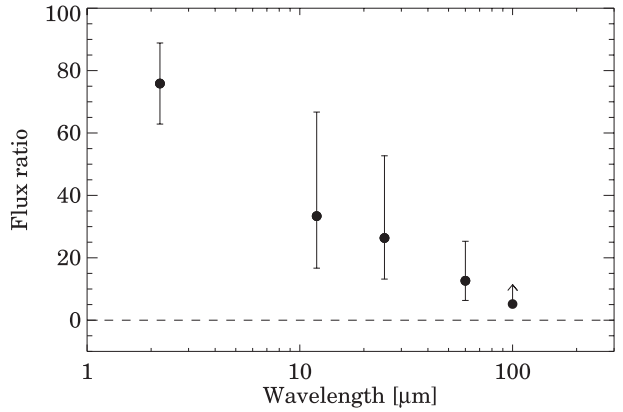

Fig. 6. Initial rise: flux ratio of peak brightness to preoutburst brightness at each wavelength. (See discussion in Sect. 3.4.2.)

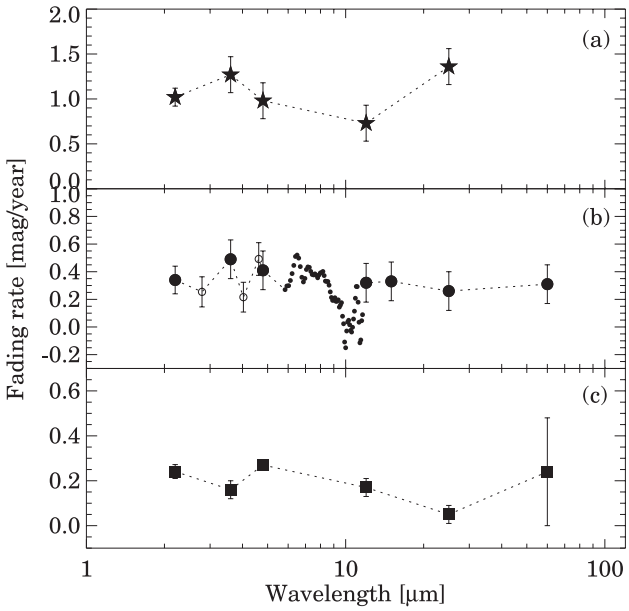

Fig. 7. Fading rates of OO Ser at different wavelengths, **a)** between 1996 April and 1996 September, **b)** between 1996 October and 1997 March, **c)** between 1997 April and 2004.

the flux increase has a characteristic wavelength dependence: the flux ratio is lower at longer wavelengths, with an approximately linear dependence on $\log \lambda$. Although the peak brightness did not occur simultaneously at different wavelengths, this trend can also be seen if one compares in Fig. 3 the preoutburst SED with the SED from 1996 September (close to peak brightness). We note that this result is different from the case of another young eruptive star, V1647 Ori, where the initial rise was practically wavelength-independent (Ábrahám et al. 2004b; Muzerolle et al. 2005).

3.4.3. The first part of the fading (until mid-1996)

During the first year after peak brightness, OO Ser exhibited similar exponential fading at all wavelengths. This can be quantified by fitting a linear relationship to the first part of the light curves plotted logarithmically in Fig. 5, using data taken only after peak brightness at a given wavelength. The derived fading rates are displayed in Fig. 7a. This graph shows that the fading rate during this period was approximately 1.0 ± 0.3 mag/year irrespectively of wavelength in the whole mid-infrared regime.

3.4.4. The second part of the fading (until mid-1997)

The second part of the light curves (between 1996 October and 1997 September) can be characterised by fading rates of 0.35 ± 0.10 mag/year, similar at all wavelengths from 2.2 to 60 μm (Fig. 7b). This is approximately three times slower than the fading during the first part. In this period ISOPHOT-S spectra were also obtained, which give the opportunity to analyse the fading with high wavelength resolution. In order to increase the signal-to-noise ratio, the fitted fading rates of ISOPHOT-S were binned (in the case of the short wavelength channels) or smoothed (in the case of the long-wavelength channels). The resulting values are overplotted with small open or filled dots in Fig. 7b, respectively. These values also support a wavelength-independent fading, characteristic of the second part of the outburst (except where the emission of OO Ser is strongly reduced by the silicate absorption around 10 μm, introducing a large uncertainty in the fit).

3.4.5. The third part of the fading (until 2004)

New measurements from 2004 revealed that the fading monitored by ISOPHOT continued at all wavelengths after 1997. We calculated fading rates for the period 1997−2004. The resulting numbers, which are plotted in Fig. 7c, are even lower than those for the second part and they also show no wavelength dependence. The values are in the range of 0.19 ± 0.08 mag/year.

3.4.6. The present status of OO Ser

In Fig. 5 the preoutburst fluxes (marked by dashed lines) can be compared with the latest measurements from 2004−2006. This comparison reveals that in 2004 OO Ser was still above the preoutburst state in the whole infrared wavelength regime, indicating that the outburst had not finished yet. The same conclusion can be drawn from Fig. 3 if one compares the SED from 1996 with that from 2004.

In Fig. 5 the last K-band photometric point from 2006 seems to deviate from a linear extrapolation of the preceding fading, possibly indicating a fourth phase of the outburst with very slow flux change. Extrapolating the lightcurves using the rates calculated for the third part of the fading (1997−2004), the expected end date of the outburst is ≈2011 from both the 2.2 μm and the 12 μm lightcurve. The slowing down of the fading process, however, may delay this event even well beyond 2011.

3.5. K-band spectral evolution

Figure 2 displays our K-band spectrum from 2006, together with the outburst spectra from 1995 and 1998 (Hodapp 1999). All three spectra are taken with comparable slit widths and were normalised to their value at 2.4 μm. In general, all spectra show a steep continuum, rising towards longer wavelengths. No individual absorption or emission lines can be seen. The overall shape of the three spectra is very similar, though there is a tendency that later spectra are less steep.

4. Discussion

4.1. The outburst

OO Ser offers a unique possibility to investigate the long-term behaviour of an eruptive young stellar object. The rise time of OO Ser was 8.5 months at the longest (Hodapp et al. 1996b),

similar to the typical timescale of "fast" FUor outbursts (e.g. the outburst of FU Ori or V1057 Cyg, which was modelled by a triggered eruption, see Bell et al. 1995).

As discussed in Sect. 3.4.1, the fading rate abruptly decreased 350 days after the maximum brightness. A similar event was observed in the case of V1057 Cyg (Kenyon & Hartmann 1991) too, but there the transition happened later, about 1300 days after the maximum. Using the light curves of Kenyon & Hartmann (1991) we computed fading rates for V1057 Cyg and compared them with corresponding values of OO Ser. We found that both before and after the transition, the fading of OO Ser (1.00 mag/yr before, 0.35 mag/yr after) was significantly faster than that of V1057 Cyg (0.09...0.40 mag/yr before, 0.04...0.14 mag/yr after, between 0.44 and 21 μm).

From the 2.2 μm light curve in Fig. 5 we can conclude that the object will return to the quiescent phase some time after 2011. This implies that the duration of the outburst of OO Ser will be at least 16 years. This timescale differs both from that of FUors (being several decades or a century) and that of EXors (being some weeks or months), suggesting that OO Ser is a young eruptive object that differs from both FUors and EXors.

The magnitude of the luminosity change during outburst is another argument in favour of OO Ser being different from FUors or EXors. From Fig. 3 we could estimate a bolometric preoutburst luminosity of $L_{\rm pre} = 4.5 \pm 1.5\ L_{\odot}$ for OO Ser and from the ISOPHOT data we also computed luminosities for OO Ser for the different epochs during the outburst. Since the far-infrared fluxes are contaminated by nearby sources, we calculated an upper and a lower limit for the luminosity, by including or neglecting the 100–200 μm data points, respectively. Adopting the 1996 February values of $L_{\rm peak} = 26 \ldots 36\ L_{\odot}$ as a representative outburst luminosity range, OO Ser changed its luminosity by a factor of about 6 . . . 8. Thus one may conclude that both the peak brightness and the amplitude of the luminosity increase was significantly lower than the corresponding values of classical FUors ($\sim$100 $L_{\odot}$ and a factor of 100, see Hartmann & Kenyon 1996).

We note that there exists another star, V1647 Ori, which seems to share some characteristics of OO Ser. Based on the amplitude of its brightening, V1647 Ori was classified as an intermediate-type object between FUors and EXors by Muzerolle et al. (2005). Preoutburst and outburst luminosities of V1647 Ori are $L_{\rm pre} = 5.6\ L_{\odot}$ (Ábrahám et al. 2004b) and $L_{\rm peak} = 44\ L_{\odot}$ (Muzerolle et al. 2005), respectively, thus its luminosity changed by a factor of about 8, similarly to OO Ser. The timescales of their outbursts are somewhat different, because the eruption of V1647 Ori was only 2 years long (Kóspál et al. 2005) and it also produced an outburst in the 1960s (Aspin et al. 2006).

We speculate, following Hodapp et al. (1996b), that OO Ser (and in some respects V1647 Ori) may be the representative of a new class of young eruptive stars ("Deeply Embedded Outburst Star" or DEOS in Hodapp et al. 1996b). Members of this class may be defined by their relatively short timescales compared to FUors, possibly recurrent outbursts, modest increase in bolometric luminosity and accretion rate, and an evolutionary state earlier than that of typical FUors or EXors (see Sect. 4.2).

4.2. The evolutionary stage of OO Ser

Based on optical to millimetre measurements available at that time, Hodapp et al. (1996b) claimed that the SED of OO Ser appeared consistent with that of a class I source and assumed its age to be 10^5 yr, indicating that OO Ser is in a very early evolutionary phase. The new data presented in this paper make it possible to reestablish the evolutionary stage of the source. We followed the method of Chen et al. (1995) and computed the bolometric temperature $T_{\rm bol}$ according to their Eq. (1) for the preoutburst, outburst and present SEDs. Due to the uncertainty of the far-infrared data points (see Sect. 2.7 about source confusion), we calculated $T_{\rm bol}$ in two different ways, with and without data points affected by source confusion ($60 < \lambda < 800\,\mu$m). The resulting values are in the range of 50–120 K for all three SEDs. Within this interval, the bolometric temperature slightly increased, and the luminosity changed by a factor of 7 during the outburst. We compared these values with the distribution of corresponding values among young stellar objects in the Taurus and ρ Ophiuchus star forming regions (Chen et al. 1995). From this check we can conclude that OO Ser seems to be an early class I object, and its age is $<10^5$ yr.

4.3. Structure of the circumstellar environment

The circumstellar environment of young eruptive stars is usually modelled with a flat or flared accretion disc and an extended infalling envelope (e.g. Kenyon & Hartmann 1991; Turner et al. 1997). In these models the emission of the central source (the star and the innermost part of the accretion disc) dominates the emission at optical and near-infrared wavelengths. Between 3 and 10 μm the origin of the emission is the release of accretion energy in the disc, and also starlight reprocessed in the same part of the disc and also in the envelope. The emission at $\lambda > 10\,\mu$m is starlight reprocessed in the envelope. The outburst occurs when, due to thermal instability in the inner edge of the disc, the accretion rate suddenly increases. After peak brightness, the accretion slowly relaxes to its quiescent value. The decreasing accretion rate causes the fading of the central source and consequently leads to the simultaneous fading of the reprocessing envelope. Thus, this model predicts a wavelength-independent fading of the source in the whole optical to mid-infrared regime (see e.g. V1057 Cyg in Ábrahám et al. 2004a and V1647 Ori in Acosta-Pulido et al. 2007).

The circumstellar environment of OO Ser probably shares many properties with the abovementioned models, except that the unusually high extinction indicates a larger and/or denser envelope. As it can be seen in Fig. 7, the fading of OO Ser was indeed wavelength-independent in the whole near- to mid-infrared wavelength regime, in agreement with the model predictions. This, together with the overall shape of its SED and the ice features in its mid-infrared spectrum indicates that the circumstellar structure of OO Ser is similar to those of other young eruptive stars, i.e. possesses a circumstellar accretion disc and is embedded in a dense circumstellar envelope.

4.4. Viscosity

Bell & Lin (1994) modelled FUor outbursts as self-regulated accretion events in protostellar accretion discs. In this model the risetime of the outburst, the subsequent high state and the time between successive outbursts are dependent on α, the viscosity parameter in the model of Shakura & Sunyaev (1973). Fitting their model to the observed FUor timescales, Bell & Lin (1994) derived $\alpha_{\rm c} = 10^{-4}$ for the α value in the cool, neutral state, and $\alpha_{\rm h} = 10^{-3}$ in the hot, ionised state. Since in many respects OO Ser is similar to FUors, the model of Bell & Lin (1994) might be applicable, although the timescales of the OO Ser outburst are remarkably shorter than that of FUors. Thus, applying this model to OO Ser requires different parameters than those

for FUors. Bell & Lin (1994) give in their Table 2 the dependence of different timescales on α, from which we can estimate $\alpha_{\rm h} = 10^{-2}$ for OO Ser. This is one order of magnitude higher than the usual value for FUors, which implies that OO Ser may differ from classical FUors in a way that its disc has different, one order of magnitude higher viscosity.

5. Summary and conclusions

In this paper we presented an infrared monitoring programme on OO Ser, a deeply embedded young eruptive star in the Serpens NW star-forming region. OO Ser went into outburst in 1995 and has been gradually fading since then. Our infrared photometric data obtained between 1996 and 2006 revealed that the fading of the source is still ongoing in the whole infrared wavelength regime, and that OO Ser will probably not return to quiescent state before 2011. The flux decay has become slower since the outburst peak and has been practically wavelength-independent.

From these results we draw the following conclusions:

- The outburst timescale and the moderate luminosity suggest that OO Ser is different from both FUors and EXors, and shows some similarities to the recently erupted young star V1647 Ori.
- Based on its SED and bolometric temperature, OO Ser seems to be an early class I object, with an age of $<10^5$ yr. As proposed by outburst models, the object is probably surrounded by an accretion disc and a dense envelope. This picture is also supported by the wavelength-independence of the fading.
- Due to the shorter timescales, outburst models developed for FUors can only work for OO Ser if the viscosity parameter in the circumstellar disc, α, is set to an order of magnitude higher value than usual for FUors.

Acknowledgements. The ISOPHOT data presented in this paper were reduced using the ISOPHOT Interactive Analisys package PIA, which is a joint development by the ESA Astrophysics Division and the ISOPHOT Consortium, lead by the Max-Planck-Institut für Astronomie (MPIA). We thank Gaspare Lo Curto for kindly providing us with the TIMMI2 data on OO Ser. We also thank the referee, Klaus Hodapp, for useful suggestions that greatly improved the paper. The work was partly supported by the grant OTKA K 62304 of the Hungarian Scientific Research Fund. J.A.P. acknowledge support from grant AYA 2001-1658, financed by the Spanish Dirección General de Investigación.

References

Ábrahám, P., Kóspál, Á., Csizmadia, S., et al. 2004a, A&A, 428, 89
Ábrahám, P., Kóspál, Á., Csizmadia, S., et al. 2004b, A&A, 419, L39
Acosta-Pulido, J. A., Kun, M., Ábrahám, P., et al. 2007, AJ, 133, 2020
Acosta-Pulido, J. A., Ballesteros, E., Barreto, M., et al. 2003, ING Newsl., 7, 15
Aspin, C., Barbieri, C., Boschi, F., et al. 2006, AJ, 132, 1298
Bell, K. R., & Lin, D. N. C. 1994, ApJ, 427, 987
Bell, K. R., Lin, D. N. C., Hartmann, L. W., & Kenyon, S. J. 1995, ApJ, 444, 376
Blommaert, J. A. D. L., Siebenmorgen, R., Coulais, A., et al., ed. 2003, The ISO Handbook, Volume II - CAM - The ISO Camera
Cesarsky, C. J., Abergel, A., Agnese, P., et al. 1996, A&A, 315, L32
Chen, H., Myers, C. P., Ladd, E. F., & Wood, D. O. S. 1995, ApJ, 445, 377
Draine, B. T. 2003, ARA&A, 41, 241
Frieswijk, W. F., Shipman, R. F., & Lahuis, F. 2004, `http://ida.esac.esa.int:8080/hpdp/technical_reports/technote12.pdf`
Gabriel, C., et al. 1997, Proc. of the ADASS VI Conference, ASP Conf. Ser., 125, 108
Hartmann, L. W., & Kenyon, S. J. 1996, ARA&A, 34, 207
Hodapp, K.-W. 1999, AJ, 118, 1338
Hodapp, K.-W., Hora, J. L., Hall, D. N. B., et al. 1996a, New Astron., 1, 177
Hodapp, K.-W., Hora, J. L., Rayner, J. T., Pickles, A. J., & Ladd, E. F. 1996b, ApJ, 468, 861
Hurt, R. L., & Barsony, M. 1996, ApJ, 460, L45
Juhász, A., Prusti, T., Ábrahám, P., & Dullemond, C. P. 2007, MNRAS, 374, 1242
Kaas, A. A., Olofsson, G., Bontemps, S., et al. 2004, A&A, 421, 623
Kenyon, S. J., & Hartmann, L. W. 1991, ApJ, 383, 664
Kessler, M. F., Steinz, J. A., Anderegg, M. E., et al. 1996, A&A, 315, L27
Kóspál, Á., Ábrahám, P., Acosta-Pulido, J., et al. 2005, IBVS, 5661, 1
Larsson, B., Liseau, R., Men'shchikov, A. B., et al. 2000, A&A, 363, 253
Laureijs, R. J., Klaas, U., Richards, P. J., Schulz, B., & Ábrahám, P., ed. 2003, The ISO Handbook, Volume IV - PHT - The Imaging Photo-Polarimeter
Lemke, D., Klaas, U., Abolins, J., et al. 1996, A&A, 315, L64
Manchado, A., et al. 2004, Proc. SPIE, 5492, 1094
Muzerolle, J., Megeath, S. T., Flaherty, K. M., et al. 2005, ApJ, 620, L107
Ott, S., et al. 1997, Proc. of the ADASS VI Conference, ASP Conf. Ser., 125, 34
Shakura, N. I., & Sunyaev, R. A. 1973, A&A, 24, 337
Tuffs, R. J., & Gabriel, C. 2003, A&A, 410, 1075
Turner, N. J. J., Bodenheimer, P., & Bell, K. R. 1997, ApJ, 480, 754

Online Material

Table 1. Log of ISOPHOT and ISOCAM observations. SP stands for spectrophotometry. "Map size" indicates the sizes of the final maps. Δ denotes the increment between adjacent pixel positions in the map (mapping) or the separation between source and background positions (ON/OFF). At certain wavelengths the beam contained nearby sources; for a detailed discussion see Sect. 2.7. All fluxes are colour corrected. The last two columns give the uncertainties of the absolute and the relative flux calibration (Sect. 2.2).

Date	ISO_id	λ [μm]	Aper./pix. size [″]	Obs. mode	Map size	Δ [″]	Flux [Jy]	Abs. unc.	Rel. unc.
1996 Feb. 28	10300901	3.6	13.8	Mapping	3×3	50×50	0.141	40%	11%
	10300901	4.8	18	Mapping	3×3	50×50	1.08	40%	1%
	10300901	12	52	Mapping	3×3	50×50	4.43	40%	25%
	10300902	25	52	Mapping	3×3	50×50	29.5	10%	10%
1996 Apr. 14	14901404	3.6	13.8	Mapping	3×1	55	0.125	40%	10%
	14901404	4.8	18	Mapping	3×1	55	0.99	40%	3%
	14901404	12	52	Mapping	3×1	55	4.07	40%	3%
	14901405	25	52	Mapping	3×1	55	39.5	10%	3%
1996 Sep. 01	29000208	3.6	13.8	Mapping	3×1	55	0.090	40%	8%
	29000208	4.8	18	Mapping	3×1	55	0.69	40%	4%
	29000208	12	52	Mapping	3×1	55	3.18	40%	5%
	29000208	15	52	Mapping	3×1	55	5.10	40%	14%
	29000210	60	43×43	Mapping	9×3	43×43	100	17%	–
	29000210	100	43×43	Mapping	9×3	43×43	116	19%	–
	29000212	200	89×89	PHT32 map	27×20	30×30	203	11%	–
	29000213	2–12	24×24	SP	3×1	45	–	–	–
1996 Oct. 06	32500703	170	89×89	PHT32 map	5×8	90×46	162	15%	–
1996 Oct. 24	34300314	3.6	13.8	Mapping	3×1	55	0.073	40%	–
	34300314	4.8	18	Mapping	3×1	55	0.62	40%	–
	34300314	12	52	Mapping	3×1	55	3.73	40%	–
	34300314	15	52	Mapping	3×1	55	4.89	40%	–
	34300315	25	52	Mapping	3×1	55	21.1	10%	–
	34300316	60	43×43	Mapping	9×3	43×43	101	16%	–
	34300316	100	43×43	Mapping	9×3	43×43	122	21%	–
	34300318	2–12	24×24	SP	3×1	45	–	–	–
1997 Mar. 08	47800219	3.6	13.8	Mapping	3×1	55	0.076	40%	10%
	47800219	4.8	18	Mapping	3×1	55	0.53	40%	5%
	47800219	12	52	Mapping	3×1	55	2.98	40%	2%
	47800219	15	52	Mapping	3×1	55	4.50	40%	3%
	47800220	25	52	Mapping	3×1	55	18.5	10%	2%
	47800221	60	43×43	Mapping	9×3	43×43	88.2	16%	–
	47800221	100	43×43	Mapping	9×3	43×43	124	20%	–
	47800223	2–12	24×24	SP	3×1	45	–	–	–
1997 Apr. 12	51301125	3.6	13.8	Mapping	3×1	55	0.060	40%	8%
	51301125	4.8	18	Mapping	3×1	55	0.61	40%	4%
	51301125	12	52	Mapping	3×1	55	3.25	40%	6%
	51301125	15	52	Mapping	3×1	55	4.20	40%	4%
	51301126	25	52	Mapping	3×1	55	18.9	10%	2%
	51301127	60	43×43	Mapping	9×3	43×43	85.3	15%	–
	51301127	100	43×43	Mapping	9×3	43×43	121	19%	–
	51301124	200	89×89	PHT32 map	27×20	30×30	233	13%	–
	51301129	2–12	24×24	SP	3×1	45	–	–	–
1997 Sep. 22	67601730/31	4.8	18	ON/OFF	-	55	0.44	40%	–
	67601730/31	12	52	ON/OFF	-	55	2.03	40%	–
	67601730/31	15	52	ON/OFF	-	55	3.76	40%	–
	67601730/31	25	52	ON/OFF	-	55	17.1	10%	–
	67601732	60	43×43	Mapping	9×3	43×43	82.9	16%	–
	67601732	100	43×43	Mapping	9×3	43×43	118	20%	–
	67601734	2–12	24×24	SP	3×1	45	–	–	–
	67601735	6.7	1.5×1.5	ISOCAM	44×44	1.5×1.5	0.712	3.3%	–
	67601735	14.3	1.5×1.5	ISOCAM	44×44	1.5×1.5	3.53	4.8%	–

Table 2. Log of observations from 2004–2006. All fluxes are presented in mJy. Spitzer fluxes are from the third delivery of data from the "c2d" legacy project, except the 70 μm data of all sources and the 3.6, 4.5, 5.8, 8 and 24 μm data of OO Ser, which were extracted by us from MIPS and IRAC images improved and published by the "c2d" legacy team. All Spitzer fluxes are colour corrected.

λ [μm]	Date	Instrument	OO Ser	V370 Ser	V371 Ser	EC 38	SMM 9
2.2	2004 Jun. 11	LIRIS	1.16 ± 0.20	2.25 ± 0.39	3.76 ± 0.57	5.64 ± 0.95	0.13 ± 0.02
2.2	2006 May 6	LIRIS	1.54 ± 0.26	2.85 ± 0.44	1.60 ± 0.22	4.82 ± 0.70	0.15 ± 0.02
3.6	2004 Apr. 4	IRAC	7 ± 1	17 ± 1	10 ± 1	43.4 ± 0.4	1.9 ± 0.2
4.5	2004 Apr. 4	IRAC	82 ± 2	38 ± 1	17 ± 1	101 ± 1	3.1 ± 0.2
5.8	2004 Apr. 4	IRAC	81 ± 4	63 ± 1	140 ± 2	139 ± 1	12.4 ± 0.7
8.0	2004 Apr. 4	IRAC	570 ± 20	86 ± 2	190 ± 6	162 ± 2	14.4 ± 0.4
12	2004 Oct. 21	TIMMI2	640 ± 100	180 ± 30	–	–	–
24	2004 Apr. 5	MIPS	13 300 ± 1800	1560 ± 60	1010 ± 20	530 ± 10	227 ± 10
70	2004 Apr. 5	MIPS	14 000 ± 600	900 ± 600	7900 ± 220	5200 ± 1 400	13 400 ± 4000